JACS
JOURNAL OF THE AMERICAN CHEMICAL SOCIETY

Communication

pubs.acs.org/JACS

pH-Dependent Population Shift Regulates BACE1 Activity and Inhibition

Christopher R. Ellis and Jana Shen*

Department of Pharmaceutical Sciences, School of Pharmacy, University of Maryland, Baltimore, Maryland 21201, United States

Supporting Information

ABSTRACT: BACE1, a major therapeutic target for treatment of Alzheimer's disease, functions within a narrow pH range. Despite tremendous effort and progress in the development of BACE1 inhibitors, details of the underlying pH-dependent regulatory mechanism remain unclear. Here we elucidate the pH-dependent conformational mechanism that regulates BACE1 activity using continuous constant-pH molecular dynamics (MD). The simulations reveal that BACE1 mainly occupies three conformational states and that the relative populations of the states shift according to pH. At intermediate pH, when the catalytic dyad is monoprotonated, a binding-competent state is highly populated, while at low and high pH a Tyr-inhibited state is dominant. Our data provide strong evidence supporting conformational selection as a major mechanism for substrate and peptide-inhibitor binding. These new insights, while consistent with experiment, greatly extend the knowledge of BACE1 and have implications for further optimization of inhibitors and understanding potential side effects of targeting BACE1. Finally, the work highlights the importance of properly modeling protonation states in MD simulations.

The β-site amyloid precursor protein (APP) cleavage enzyme (β-secretase or BACE1) is an aspartyl protease that catalyzes the cleavage of APP to generate β-amyloid (Aβ) peptides.[1] Subsequent oligomerization and aggregation of Aβ are linked to the onset of Alzheimer's disease (AD).[2] While a complete understanding of the physiological roles of BACE1 has yet to be achieved,[3] BACE1-deficient mice demonstrate significantly reduced levels of Aβ and few phenotypical abnormalities.[4a,b] Thus, blocking the enzymatic activity of BACE1 has emerged as a major avenue in drug development efforts toward the treatment of AD.[4c]

Over the past 15 years since the discovery of BACE1, hundreds of inhibitors have been synthesized, and dozens have entered clinical trials, including Merck's MK8931 and AstraZeneca's AZD3293, which are currently in phase II/III trials.[5] Despite the enormous effort and progress in the development of inhibitors, the fundamental biology of BACE1, such as its physiological substrates and regulatory mechanism, is not fully understood.[3] Such knowledge, however, has implications for the prediction of side effects and further optimization of BACE1 inhibitors and the discovery of new AD targets.

BACE1 is a monomeric protein primarily localized in the endosome and trans-Golgi apparatus. The catalytic domain of BACE1 contains about 400 residues, among which two catalytic aspartates are located between the N- and C-terminal domains (Figure 1A). The aspartyl dyad hydrolyzes peptide bonds through a general acid−base mechanism in which Asp228 acts as a base to activate a bridging catalytic water while Asp32 acts as an acid to protonate the substrate carbonyl group.[6,7] Lying directly over the catalytic site is a β-hairpin loop spanning residues Tyr68 to Glu77, commonly known as the flap, that controls substrate access (Figure 1A,B). Both crystal structures and molecular dynamics (MD) simulations suggest that the flap opens and closes at room temperature.[8,9]

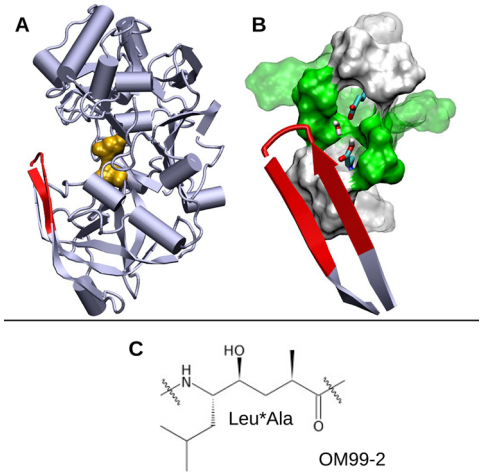

Figure 1. Structures of BACE1 and the inhibitor OM99-2. (A) Cartoon representation of *apo*-BACE1 (PDB ID 1SGZ) with the catalytic dyad (Asp32 and Asp228) colored orange and the flap (β-hairpin loop, residues 68−77) colored red. (B) Active site of BACE1. Asp32, Asp228, and bridging water are shown in stick model. Polar (green) and hydrophobic (white) residues within 5 and 7 Å of Asp32/Asp228 are depicted as solid and transparent surfaces, respectively. (C) The central hydroxyethylene group (Leu*Ala) of the peptidomimetic inhibitor OM99-2. The entire sequence is Glu-Val-Asn-Leu*Ala-Ala-Glu-Phe.

A unique aspect of the activation and inhibition of BACE1 is the delicate pH dependence. Fluorescence experiments showed that the peptide cleavage activity of BACE1 occurs in a very narrow pH range, peaking at pH 4.5 and sharply declining below pH 4 and above pH 5.[9,10] Surface plasmon resonance experiments revealed that the binding of the peptidomimetic inhibitor OM99-2 (Figure 1C) decreases as the pH increases

Received: June 7, 2015
Published: July 17, 2015

DOI: 10.1021/jacs.5b05891
J. Am. Chem. Soc. 2015, 137, 9543−9546

from 3 to 5 and is completely abolished at pH 6 and 7.[9] These observations, in conjunction with the crystal structures resolved at several pH values, led to the following hypothesis:[9] at pH 5 a conformational switch occurs, preventing substrate/inhibitor binding at high pH, while at pH 4 the active site loses the bridging water, deactivating BACE1. However, since these crystal structures have relatively low resolution (2.35−2.7 Å) and differences between them are insignificant (Table S1 in the Supporting Information (SI)), the detailed mechanism of the pH-regulated activity and binding of BACE1 remains unclear.

Here we report an atomically detailed mechanism underlying the pH-dependent enzymatic activity and inhibitor binding of BACE1 using a state-of-the-art MD technique, continuous constant-pH MD (CpHMD),[11a−c] which allows simultaneous titration of all ionizable sites in response to the conformational dynamics of the protein at a specified pH (see a recent review[11d]). CpHMD simulations with pH replica-exchange were performed on BACE1 and its complex with the inhibitor OM99-2 starting from the respective crystal structures (PDB ID 1SGZ and 1FKN) using CHARMM (version C37b).[12] The particular CpHMD used in this study employs a hybrid-solvent scheme that combines the accuracy of conformational sampling in explicit solvent with the efficiency of evaluating solvation forces on the titration coordinates by the generalized Born model.[11c] *apo*-BACE1 was simulated using 24 pH replicas in the pH range 1−8, while the holo form was simulated using 32 pH replicas at pH −0.5 to 9.0. The apo and holo proteins were simulated for 21 and 11 ns per replica, respectively, under *NPT* conditions. Detailed simulation protocols and parameters are provided in the SI. Convergence tests are presented in Figures S1−S7.

To elucidate the catalytic roles of Asp32 and Asp228, we examined their titration and solvent environment. Asp32 and Asp228 display very different titration behavior, with calculated pK_a's of 4.1 and 1.9, respectively (Figure 2A, solid lines). The first solvation shell of each Asp (total hydration number, N_h) contains approximately two water molecules at pH below 3, one of which is a bridging water (Figure 2B, solid lines). As the pH increases to 3−5.5, coinciding with the titration range of Asp32, N_h increases to just above 3, while the number of bridging waters remains constant. The increase in hydration is due to deprotonation of Asp32, which induces a conformational rearrangement of the active site and consequently water entrance, a phenomenon previously observed for other proteins such as staphylococcal nuclease in both experimental[13a] and simulation studies.[13b] As the pH further increases, there is no change in N_h, as expected, since each Asp remains deprotonated.

For *holo*-BACE1, the titration curve of Asp32 is shifted to higher pH, while that of Asp228 is shifted to lower pH (Figure 2A, dashed lines). The resulting pK_a's are 5.6 and 1.0, which are 1.5 higher and 0.9 lower than the respective apo-state values as a result of H-bonding with the hydroxyl group of Leu*Ala. The presence of the inhibitor precludes water from entering the active site when the catalytic dyad is in the monoprotonated state (Figure 2B, dashed lines). However, as Asp32 begins to deprotonate, water starts to enter, analogous to the scenario for the apo protein. Interestingly, in lieu of the bridging water, the hydroxyl group of Leu*Ala H-bonds to either Asp32 or Asp228 (Figure 2C). At pH below 4, Leu*Ala exclusively H-bonds with Asp228. As the pH increases, Asp32 starts to deprotonate, resulting in sharing of the H-bond between the two Asp's. Finally, when the pH is above 7, Asp32 becomes fully deprotonated and the exclusive H-bond acceptor.

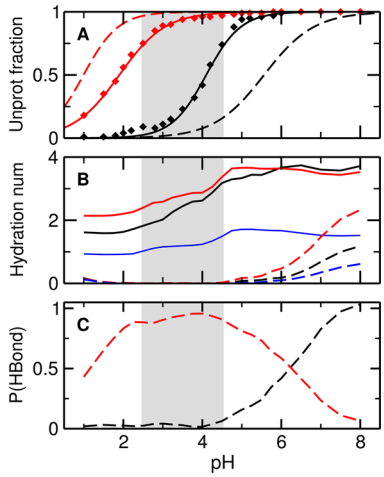

Figure 2. Simulated titration and solvent accessibility of the catalytic dyad in BACE1. (A) Unprotonated fractions of Asp32 (black) and Asp228 (red) in the apo (solid) and holo (dashed) states at different pH. The curves are the best fits to the Hill equation. (B) Hydration numbers of Asp32 (black) and Asp228 (red) and the number of bridging waters (blue). Dashed lines represent the holo state. Hydration number refers to the number of water molecules within the first solvation shell, which is defined as any water oxygen within 3.5 Å of the Asp carboxylate oxygen. (C) Occupancies of the H-bonds between the OH group of Leu*Ala in OM99-2 and Asp32 (black) and Asp232 (red). The H-bond was considered to be present if the donor−acceptor distance was below 3.5 Å and the acceptor−donor−H angle was less than 30°. Gray areas indicate the simulated active pH range.

Our calculated site-specific pK_a's are in agreement with the consensus that Asp32 and Asp228 are the acid and base, respectively, in the enzymatic reaction,[6,9] although the macroscopic pK_a's of 4.1 and 1.8 (Figure S8) are 1.1 and 1.7 units lower than the respective values inferred from a kinetic experiment (5.2 and 3.5).[6] The discrepancy can be attributed to the implicit-solvent model, which underestimates desolvation free energies.[14] Thus, the active pH range, characterized by a monoprotonated catalytic dyad, is approximately 2.5−4.5 (Figure 2, gray area), one pH unit below the experimentally observed range of 3.5−5.5.[9,10] We will keep the shift in mind in the discussion of conformational changes induced by changes in the catalytic dyad protonation state. Our data also show that a bridging water is always present regardless of pH, thus supporting the hypothesis that the active site contains a bridging water that acts as the attacking water in the catalytic reaction[6] but contradicting the hypothesis that the active site may be dehydrated at highly acidic pH.[9]

Next, we examined the conformational dynamics of BACE1 at different pH (Figure 3). Following previous simulation work by others,[8,15] we used two order parameters, R and φ, to characterize the flap conformation. R is defined as the distance between Tyr71:OH and Asp32:Cγ, while φ is a pseudodihedral angle formed by Trp76:C−Val69:N−Thr72:CA−Gln73:CA. Tyr71 is an important residue on the flap, as it is conserved in all pepsin-like aspartic proteases and its orientation was found to modulate the flap conformation in BACE1.[15] φ describes the twist of the flap, where a negative twist orients the flap toward the active site and a positive twist presents a more open active site.[15]

Remarkably, the free energy surface (FES) as a function of R and φ reveals three local free energy minima (Figure 3A). We refer to these three states as the Tyr-inhibited, binding-competent, and Gln-inhibited states. In the Tyr-inhibited state, corresponding to the minimum located at R < 5 Å, Tyr71

DOI: 10.1021/jacs.5b05891
J. Am. Chem. Soc. 2015, 137, 9543−9546

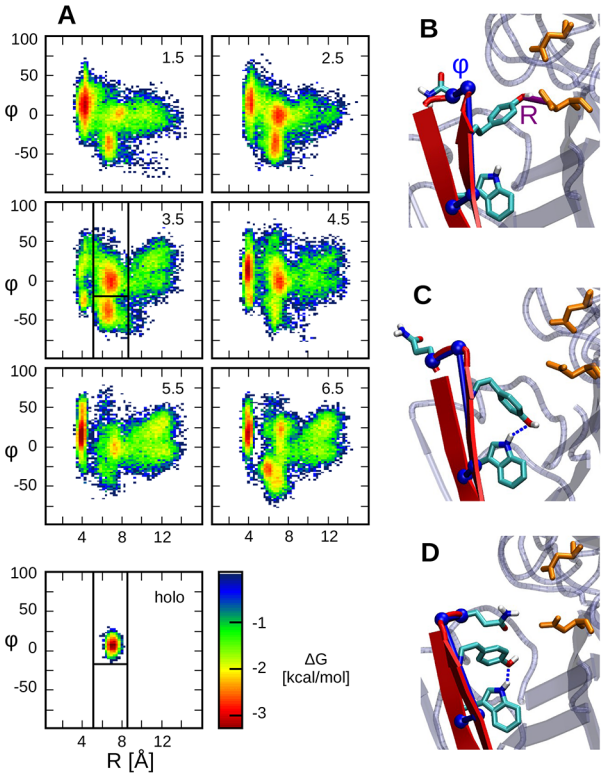

Figure 3. pH-dependent conformational states of BACE1. (A) Free energy surface of *apo*-BACE1 as a function of R and φ under various pH conditions (indicated in the upper right corners). The panel at the bottom left presents the FES of *holo*-BACE1 at pH 4.5. The free energy was calculated as $-kT \ln P(R, \varphi)$, where k is the Boltzmann constant and T is the temperature. Vertical and horizontal lines in the panel for pH 3.5 define the various states. (B–D) Representative snapshots of the (B) Tyr-inhibited, (C) binding-competent, and (D) Gln-inhibited states. The order parameters R (purple) and φ (blue) are shown.

interacts with Asp32, causing the flap to cover the active site, preventing ligand binding (Figure 3B). Similar self-inhibited states have been reported for aspartic proteases[16,17] as well as BACE1.[8,15] Separated from the Tyr-inhibited state by a barrier of about 3 kcal/mol are two states with the free energy minima located between R = 5 and 8.5 Å, one below and one above $\varphi = -18°$. In the state with $\varphi > -18°$, Tyr71 points toward the base of the flap, allowing H-bond formation with the indole group of Trp76 (Figure 3C). Importantly, this state is exclusively sampled in the holo simulations. Thus, we call it the binding-competent state. In the state with $\varphi < -18°$, Tyr71 maintains the same orientation, but because of the twist of the flap (change in φ), the side chain of Gln73 occludes the active site (Figure 3D). Thus, we call this state the Gln-inhibited state. It is noteworthy that unlike Tyr71, the distance between Gln73 and Asp32 rarely becomes short enough to induce H-bond formation (Figure S9). The free energy barrier separating the Gln-inhibited and binding-competent states is very small (<1 kcal/mol). Finally, we refer to the regions in the FES with R > 8.5 Å and no visible free energy minimum as diffuse states.

The FES reveals that *apo*-BACE1 samples distinct conformational states in a pH-dependent manner and that upon inhibitor binding only the binding-competent state is visited (Figure 3A, bottom plot). At pH below 2 or above 5, when the catalytic dyad is diprotonated or dideprotonated, the Tyr-inhibited state is dominant (Figure 3A). At pH 2.5–4.5, the simulated active pH range where the catalytic dyad is in the monoprotonated form, the binding-competent state becomes more populated (Figure 3A). More quantitative analysis will be given later. Interestingly, in the FES at pH 3.5, the Tyr-inhibited state is significantly diminished, suggesting that this is the most active pH in our simulation. This is consistent with the experimental observation that the most active pH is about 0.7 units below the pK_a of Asp32. The FES of the holo protein at all pH shows only one free energy minimum located in the same region as the binding-competent state of *apo*-BACE1. This is consistent with the fact that the crystal structures of BACE1 bound to OM99-2 obtained at pH 5 and pH 7.4 are nearly identical and supports the hypothesis that binding of OM99-2 locks BACE1 into a single conformation.[9]

To quantify the extent of the conformational switch induced by pH, the occupancies of the aforementioned states were calculated as a function of pH (Figure 4A). The occupancy of the

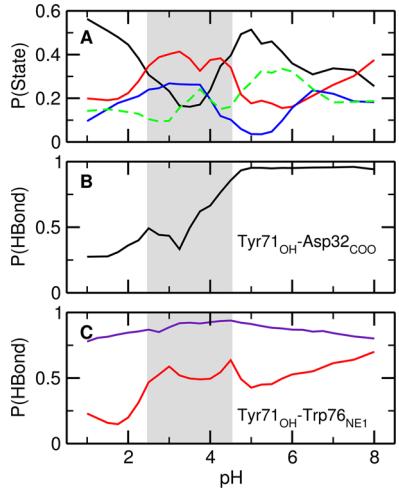

Figure 4. Characterization of the Tyr-inhibited and binding-competent states of BACE1. Occupancies of (A) the Tyr-inhibited (black), Gln-inhibited (blue), binding-competent (red), and diffuse (green) states of *apo*-BACE1, (B) the Tyr71:OH···Asp32:COO H-bond in the Tyr-inhibited state of *apo*-BACE1, and (C) the Tyr71:OH···Trp76:NE1 H-bond in the binding-competent population (red) and *holo*-BACE1 (purple) are shown. Gray areas indicate the simulated active pH range.

diffuse states remains nearly constant (about 20%) over the entire pH range, whereas the occupancies of the other three states vary dramatically. In particular, the occupancy profile of the Tyr-inhibited state has a shape complementary to those of the binding-competent/Gln-inhibited states. Thus, pH shifts the relative population between the states. Since the Gln-inhibited state has a low population (below 25% over the entire pH range) and readily converts to the binding-competent state, we will focus on the former in the discussion below.

At pH below 2, the Tyr-inhibited state has the highest occupancy, accounting for about 50% of the total population. This offers an explanation for the inactivity of BACE1 at low pH when the catalytic dyad is in the diprotonated state. As the pH increases from 2 to 3.5, the occupancy of the Tyr-inhibited state steadily decreases, whereas that of the binding-competent state steadily increases. The former reaches a minimum at about pH 3.5, while the latter reaches a broad maximum in the pH range 2.5–4.5, where it becomes the most occupied state, accounting for approximately 40% of the total population. This provides quantitative support for the active pH range of 2.5–4.5, which corresponds to the monoprotonated state of the catalytic dyad. As the pH increases from 3.5 to 5, Asp32 becomes deprotonated,

DOI: 10.1021/jacs.5b05891
J. Am. Chem. Soc. 2015, 137, 9543–9546

the occupancy of the Tyr-inhibited state increases, and that of the binding-competent state decreases, further confirming that BACE1 is most active in the monoprotonated state and explaining why the inhibitor cannot bind at pH 6 and 7.[9]

Curiously, the occupancy analysis did not resolve which state dominates the conditions of pH above 5. To understand this, we considered the occupancy of the H-bond between Tyr71 and Asp32 in the Tyr-inhibited state. Remarkably, at pH 5 and above, the H-bond is nearly 100% present (Figure 4B), indicating that at high pH when Asp32 is deprotonated, the active site can be fully occluded. Once this happens, the probability for converting to the binding-competent state is very low because of the high energy barrier (Figure 3A, pH 5.5 and 6.5). Thus, the data support the hypothesis that the self-inhibited conformation is the most stable state at high pH.[8,9] Moreover, at high pH, Asp32 is fully deprotonated and therefore unable to donate a proton to the substrate as required for catalysis.

Finally, we examined the binding-competent state by focusing on the H-bond between Tyr71 and Trp76, which is nearly always present when OM99-2 is bound (Figure 4C, purple). In *apo*-BACE1, the occupancy of this H-bond reaches a maximum at pH 2.5−4, coinciding with the pH range for the maximum occupancy of the binding-competent state (Figure 4C, red). This observation is consistent with the finding that *apo*-BACE1 readily assumes the binding-competent state in the active pH range, thus suggesting that peptide-inhibitor/substrate binding takes place, at least in part, via the conformational selection mechanism. We note that unlike OM99-2, which resembles the natural substrate, entrance of many small-molecule inhibitors requires the flap to open further, leading to the loss of the Tyr71···Trp76 H-bond.

In summary, CpHMD simulations have revealed a detailed mechanism of the pH-regulated enzymatic activity and peptide-inhibitor binding of BACE1 (Figure 5) because of the mobility of the flap, *apo*-BACE1 mainly samples two distinct states, Tyr-inhibited and binding-competent. Changes in pH shift the relative populations of the two states such that at intermediate pH, where the catalytic aspartates are in the monodeprotonated form, the binding-competent state is the most occupied. However, at both low and high pH, the Tyr-inhibited state is thermodynamically more stable, and large free energy barriers separate the states. This mechanism is consistent with the experimental observations and previous simulation studies but is somewhat different from the mechanism proposed by Shimizu et al.[9] Specifically, our simulations demonstrate that instead of dehydration of the active site at low pH, the active site remains hydrated and adopts a Tyr-inhibited state. Thus, our simulations suggest that mutation of Tyr71 to a side chain such as Phe that is incapable of H-bonding with Asp32 may significantly increase the enzyme activity, especially at high pH. Moreover, our simulations offer an unprecedented view of the interplay among pH, protonation state, H-bonding, and conformational dynamics. The resemblance between the binding-competent state of *apo*-BACE1 and the peptide-inhibitor-bound state suggests a conformational selection mechanism for binding. Finally, the present work demonstrates the utility of CpHMD in gaining novel insights into the intricacy of pH-dependent enzyme catalysis and inhibition.

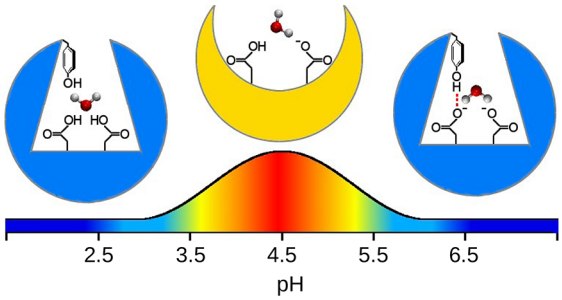

Figure 5. pH-dependent mechanism of BACE1 activity and inhibition. The active pH range has been shifted by one unit to match experiment.

■ ASSOCIATED CONTENT

Supporting Information

Details of the computational protocols and additional analyses, and complete refs 1a−c, 2b, 4a−c, and 12. The Supporting Information is available free of charge on the ACS Publications website at DOI: 10.1021/jacs.5b05891.

■ AUTHOR INFORMATION

Corresponding Author

*jshen@rx.umaryland.edu

Notes

The authors declare no competing financial interest.

■ ACKNOWLEDGMENTS

Financial support was provided by NSF (MCB1305560) and NIH (GM098818).

■ REFERENCES

(1) (a) Hussain, I.; et al. *Mol. Cell. Neurosci.* **1999**, *14*, 419−427. (b) Sinha, S.; et al. *Nature* **1999**, *402*, 537−540. (c) Vassar, R.; et al. *Science* **1999**, *286*, 735−741.

(2) (a) Hardy, J.; Selkoe, D. J. *Science* **2002**, *297*, 353−356. (b) Bateman, R. J.; et al. *N. Engl. J. Med.* **2012**, *367*, 795−804.

(3) Kandalepas, P. C.; Vassar, R. *J. Neurochem.* **2012**, *120* (Suppl. 1), 55−61.

(4) (a) Luo, Y.; et al. *Nat. Neurosci.* **2001**, *4*, 231−232. (b) Nishitomi, K.; et al. *J. Neurochem.* **2006**, *99*, 1555−1563. (c) Yuan, J.; et al. *J. Med. Chem.* **2013**, *56*, 4156−4180.

(5) Vassar, R. *Alzheimer's Res. Ther.* **2014**, *6*, 89.

(6) Toulokhonova, L.; Metzler, W. J.; Witmer, M. R.; Copeland, R. A.; Marcinkeviciene, J. *J. Biol. Chem.* **2003**, *278*, 4582−4589.

(7) Hong, L.; Tang, J. *Biochemistry* **2004**, *43*, 4689−4695.

(8) Gorfe, A. A.; Caflisch, A. *Structure* **2005**, *13*, 1487−1498.

(9) Shimizu, H.; Tosaki, A.; Kaneko, K.; Hisano, T.; Sakurai, T.; Nukina, N. *Mol. Cell. Biol.* **2008**, *28*, 3663−3671.

(10) Grüninger-Leitch, F.; Schlatter, D.; Küng, E.; Nelböck, P.; Döbeli, H. *J. Biol. Chem.* **2002**, *277*, 4687−4693.

(11) (a) Lee, M. S.; Salsbury, F. R., Jr.; Brooks, C. L., III *Proteins: Struct., Funct., Genet.* **2004**, *56*, 738−752. (b) Khandogin, J.; Brooks, C. L., III *Biophys. J.* **2005**, *89*, 141−157. (c) Wallace, J. A.; Shen, J. K. *J. Chem. Theory Comput.* **2011**, *7*, 2617−2629. (d) Chen, W.; Morrow, B. H.; Shi, C.; Shen, J. K. *Mol. Simul.* **2014**, *40*, 830−838.

(12) Brooks, B. R.; et al. *J. Comput. Chem.* **2009**, *30*, 1545−1614.

(13) (a) Damjanović, A.; Brooks, B. R.; García-Moreno E., B. *J. Phys. Chem. A* **2011**, *115*, 4042−4053. (b) Shi, C.; Wallace, J. A.; Shen, J. K. *Biophys. J.* **2012**, *102*, 1590−1597.

(14) Wallace, J. A.; Wang, Y.; Shi, C.; Pastoor, K. J.; Nguyen, B.-L.; Xia, K.; Shen, J. K. *Proteins: Struct., Funct., Genet.* **2011**, *79*, 3364−3373.

(15) Spronk, S. A.; Carlson, H. A. *Proteins: Struct., Funct., Genet.* **2011**, *79*, 2247−2259.

(16) Andreeva, N.; Dill, J.; Gilliland, G. L. *Biochem. Biophys. Res. Commun.* **1992**, *184*, 1074−1081.

(17) Gustchina, A.; Li, M.; Phylip, L. H.; Lees, W. E.; Kay, J.; Wlodawer, A. *Biochem. Biophys. Res. Commun.* **2002**, *295*, 1020−1026.

DOI: 10.1021/jacs.5b05891
J. Am. Chem. Soc. 2015, 137, 9543−9546